AGU PUBLICATIONS

Geophysical Research Letters

RESEARCH LETTER
10.1002/2017GL072884

Key Points:
- The importance of mesoscale variability in the Gulf of Mexico for the upper ocean heat budget and air-sea interactions
- Lateral ocean advective eddy fluxes support warm SST and surface turbulent heat fluxes in the Gulf of Mexico
- The importance of resolving ocean mesoscale variability in GCMs to capture the contribution of submonthly ocean lateral advection on latent heat flux into the atmosphere

Supporting Information:
- Supporting Information S1

Correspondence to:
D. A. Putrasahan,
dian.putrasahan@mpimet.mpg.de

Citation:
Putrasahan, D. A., I. Kamenkovich, M. Le Hénaff, and B. P. Kirtman (2017), Importance of ocean mesoscale variability for air-sea interactions in the Gulf of Mexico, *Geophys. Res. Lett.*, *44*, doi:10.1002/2017GL072884.

Received 1 FEB 2017
Accepted 30 MAY 2017
Accepted article online 2 JUN 2017

©2017. American Geophysical Union. All Rights Reserved.

Importance of ocean mesoscale variability for air-sea interactions in the Gulf of Mexico

D. A. Putrasahan[1,2], I. Kamenkovich[1], M. Le Hénaff[3,4], and B. P. Kirtman[1]

[1]Rosenstiel School of Marine and Atmospheric Science, University of Miami, Coral Gables, Florida, USA, [2]Max Planck Institute of Meteorology, Hamburg, Germany, [3]Cooperative Institute for Marine and Atmospheric Studies, University of Miami, Coral Gables, Florida, USA, [4]NOAA Atlantic Oceanographic and Meteorological Laboratory, Miami, Florida, USA

Abstract Mesoscale variability of currents in the Gulf of Mexico (GoM) can affect oceanic heat advection and air-sea heat exchanges, which can influence climate extremes over North America. This study is aimed at understanding the influence of the oceanic mesoscale variability on the lower atmosphere and air-sea heat exchanges. The study contrasts global climate model (GCM) with 0.1° ocean resolution (high resolution; HR) with its low-resolution counterpart (1° ocean resolution with the same 0.5° atmosphere resolution; LR). The LR simulation is relevant to current generation of GCMs that are still unable to resolve the oceanic mesoscale. Similar to observations, HR exhibits positive correlation between sea surface temperature (SST) and surface turbulent heat flux anomalies, while LR has negative correlation. For HR, we decompose lateral advective heat fluxes in the upper ocean into mean (slowly varying) and mesoscale-eddy (fast fluctuations) components. We find that the eddy flux divergence/convergence dominates the lateral advection and correlates well with the SST anomalies and air-sea latent heat exchanges. This result suggests that oceanic mesoscale advection supports warm SST anomalies that in turn feed surface heat flux. We identify anticyclonic warm-core circulation patterns (associated Loop Current and rings) which have an average diameter of ~350 km. These warm anomalies are sustained by eddy heat flux convergence at submonthly time scales and have an identifiable imprint on surface turbulent heat flux, atmospheric circulation, and convective precipitation in the northwest portion of an averaged anticyclone.

1. Introduction

Mesoscale variability in many parts of the world's ocean has a significant impact on the atmosphere in such eddy-rich regions as western boundary currents and their extensions along sea surface temperature (SST) fronts [*Putrasahan et al*., 2013; *O'Neill et al*., 2012; *Small et al*., 2008; *Siqueira and Kirtman*, 2016], Agulhas leakage [*Putrasahan et al*., 2015; *Souza et al*., 2014], and the Southern Ocean [*Frenger et al*., 2013]. For example, when air blows across an SST front toward warmer waters, it experiences heating near the surface, which causes changes in the atmospheric boundary layer and above. The resulting effects in the atmosphere include anomalous turbulent heat fluxes out of the ocean, enhanced convection and precipitation [*Czaja*, 2012], anomalous pressure gradients ("pressure adjustment mechanism") [*Lindzen and Nigam*, 1987], and intensified momentum transfer to the surface ("vertical mixing mechanism") [*Wallace et al*., 1989; *Chelton et al*., 2007]. These processes can have significant impact on the atmosphere and the air-sea interactions [e.g., *Small et al*., 2008; *Hewitt et al*., 2016]. However, current generation of global climate models (GCMs), such as those used in Coupled Model Intercomparison Project, Fifth phase, are unable to resolve mesoscale dynamics and variability due to a lack of spatial resolution in their oceanic components. This study examines air-sea interactions at the oceanic mesoscale and the importance of oceanic advection in modulating these interactions in the Gulf of Mexico (GoM), as a region of intense mesoscale variability.

Ocean dynamics in the GoM is dominated by the local portion of the North Atlantic western boundary current upstream of the Gulf Stream, called the Loop Current (LC). The LC has a variable pathway, from a retracted or port-to-port position, in which the current flows almost directly from the Yucatan Channel to the Florida Straits, to an extended position, where it interacts with the Northern GoM continental shelf break. When the LC is extended, its tip eventually closes and forms a large, warm-core anticyclone, or LC rings, which eventually separates from the LC, resulting in the immediate retraction of the LC to the port-to-port position. After separation ("shedding"), a LC ring drifts westward while slowly decaying before dissipating near the western GoM shelf. The ring shedding sequence is highly variable in duration, from 0.5 to 19 months with peaks at 6, 9, and 11.5 months [*Leben*, 2005; *Chang and Oey*, 2012]. Shedding events happen at any month during the

year, with episodes most frequently observed in early spring (March) and early autumn (September) [*Chang and Oey*, 2012]. Typical LC rings have an initial diameter ranging from 200 to 400 km, with an average value of 330 km [*Oey et al*., 2005; *Vukovich*, 2007]. The ring shedding also involves cyclonic eddies, which are observed at the LC edges and have diameters of 80 to 120 km [*Le Hénaff et al*., 2014].

Mesoscale variability in the GoM can have substantial influence on climate extremes over North America. For example, the warm-core rings in the GoM can play a potentially significant role in intensifying hurricanes passing over them, which was observed during Hurricanes Gilbert (1988) and Opal (1995) [*Shay et al*., 2000; *Jacob and Shay*, 2003] and more recently for Hurricane Katrina (2005) [*Jaimes and Shay*, 2009, 2010]. Additionally, U.S. climate is partially influenced by the regional distribution of oceanic heat anomalies associated with the Atlantic warm pool (AWP), which encompasses the Caribbean Sea, the GoM, and tropical Atlantic Ocean. This is in turn affected by the advection of heat from mesoscale oceanic currents in the Intra-Americas Sea, which connects the Caribbean to the GoM. This will have differing implications on U.S. climate impact since the oceanic heat distribution in the AWP plays an important role on rainfall distribution over the Caribbean and U.S., affecting frequency and severity of droughts and torrential rain, as well as in regulating conditions that favor formation and intensification of hurricanes [*Wang and Lee*, 2007; *Wang et al*., 2006; *Wang and Lee*, 2008]. While previous studies have shown the importance of surface heat and radiative fluxes for AWP formation in summer [*Wang and Enfield*, 2002; *Enfield*, 2005] and its associated moisture and precipitation increase over the GoM and continental U.S. [*Wang et al*., 2007] and extreme weather [*Jung and Kirtman*, 2016], the role of ocean advection is still under debate [*Lee et al*., 2007]. The uncertainty comes in large part from the lack of understanding of the role of oceanic advection in heat distribution and air-sea interactions in the region, since aforementioned key studies did not resolve the oceanic mesoscale.

In this study, we highlight the importance of ocean mesoscale variability in the GoM through a comparative study between an Intergovernmental Panel on Climate Change-class model and an eddy-resolving GCM. We will explore its effects on the distribution of heat anomalies in the GoM and their influence on ocean-atmosphere processes. Section 1 describes the model and observational data set used for this study. Section 2 provides details of the ocean circulation and variability in the GoM seen through observations and the model. This mesoscale variability is further separated into the slowly evolving LC and rings ("mean") and submonthly anomalies ("eddies"). The importance of these eddies on heat anomaly distribution and air-sea interactions is revealed in section 3. We further explore the effects of the LC meanders, rings, and eddies on the overlying atmosphere in section 4 and provide a summary of the entire study in section 5.

2. Data: Model and Observations

We use monthly averaged outputs from two simulation runs of the Community Climate System Model version 4 (CCSM4), which is a global coupled climate model composed of the Community Land Model version 4, the Community Atmospheric Model version 4, the Los Alamos Parallel Ocean Program version 2 ocean general circulation model, and the Community Ice Code version 4, with each model component communicating via the CCSM flux coupler. Both simulations have atmospheric and land components of the same 0.5° resolution (0.625° zonal and 0.5° meridional) but differ on ocean and sea-ice resolution, with the high-resolution case (HR) using 0.1° resolution while the low-resolution case (LR) uses 1° resolution. HR has been shown to capture frontal air-sea interactions that have important climate implications [*Putrasahan et al*., 2015; *Siqueira and Kirtman*, 2016; *Kirtman et al*., 2012; *McClean et al*., 2011; *Bryan et al*., 2010]. The analysis described in this study is based on 54 years of HR simulations and 99 years of LR simulations. The 54 years of the HR simulation follows 100 years of spin-up, and details of the model experiments and setup have been previously documented in *Kirtman et al*. [2012].

Satellite observations and reanalysis products are used to identify air-sea coupling and verify model outputs. We use ocean geostrophic velocity estimates from Archiving, Validation, and Interpretation of Satellite Oceanographic data (AVISO) altimetry products (DUACS 2014), for the period 1993–2014. AVISO maps of geostrophic currents have a 0.25° resolution and are estimated daily. We utilize daily 0.25° SST products from the Group of High Resolution Sea Surface Temperature (GHRSST) for the period of 1982–2014 [*Reynolds et al*., 2007] and corresponding monthly 1° latent heat flux estimates from the Woods Hold Oceanographic Institution Objectively Analyzed Air-Sea Heat Fluxes project [*Yu and Weller*, 2007].

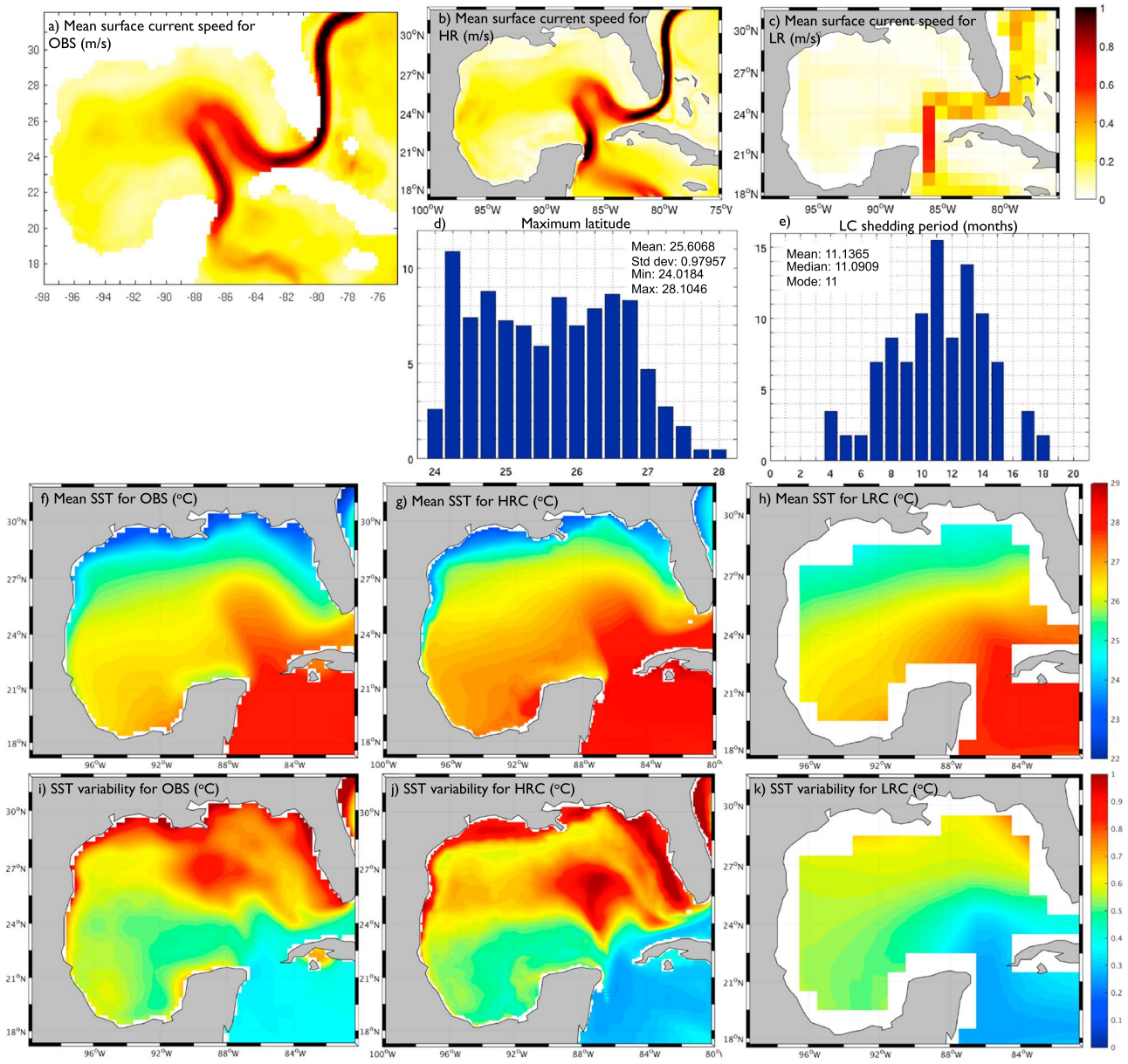

Figure 1. Climatological mean surface current speed (m/s) from (a) satellite observations, (b) HR, and (c) LR. Histograms from HR simulation of the (d) LC most northern latitude distribution and (e) LC shedding period distribution in months. Climatological mean SST (°C) from (f) GHRSST, (g) HR, and (h) LR. Root-mean-square of SST (°C) from (i) GHRSST, (j) HR, and (k) LR.

3. Circulation and Mesoscale Variability

The time-mean currents from the LR (99 years) and HR (54 years) simulations, as well as the mean geostrophic current estimated from altimetry (1993–2014), are shown in Figures 1a–1c. The LC flows along a nearly fixed path in the Yucatan Channel, Florida Straits and the Atlantic Ocean, mainly because of topographic constraints. As a result, the time average of the currents is intense in these regions. In contrast, the LC path is highly variable upstream and inside the GoM, and this variability manifests itself in time-mean fields as a broad flow between approximately 23°N and 27°N. HR exhibits a very realistic mean current in terms of location and intensity, compared to observations. In contrast and as expected, LR exhibits a very broad, weak, and nearly stationary LC, which does not extend into the northern GoM and is locked in the port-to-port position.

We next analyze the variability in model-simulated sea surface height (SSH) and compare it to literature estimates in *Leben* [2005] that is based on 12 years of altimetry data. As in *Leben* [2005], we defined the LC

contour inside the GoM by the 17 cm SSH anomaly over the basin mean and its northern extension as the most northern latitude of the LC streamline at each moment. The resulting distribution of the LC northern extension (Figure 1d) has a mean value of 25.6°N, slightly more southward than the value of 26.2°N in observations. This is due to a tendency of the HR-simulated LC to be in the port-to-port situation, which can be seen as the main peak in the distribution histogram. The secondary peak is, however, close to 26.5°N, which is the main peak observed in altimetry. The standard deviation in the HR-simulated LC extension is 0.97°, which is almost identical to the observed value of 0.95°. The minimum and maximum values of the LC latitude in the HR simulation are 24°N and 28.1°N, almost identical to the observed values [*Dukhovskoy et al*., 2015].

The LC ring shedding events, that is, the separation of a LC ring and the southward retraction of the LC, are studied next. The shedding periods are defined as intervals between two consecutive shedding events. The distribution of the shedding period for the HR simulation (Figure 1e) has a main peak at 11 months, which is close to the mean value, and a secondary peak at 13 months. These values are a little longer than in observations. The distributions derived by *Leben* [2005] from altimetry data for the 1993–2003 period, and by *Chang and Oey* [2012] using altimetry data for the 1993–2010 period and in situ estimates and remote sensing for the period 1974–1992, show peaks at 6 and 9 months. However, the shedding periods derived in the HR simulation range from 4 to 18 months, which is well within the observed range between 0.5 and 19 months [*Leben*, 2005; *Chang and Oey*, 2012]. Overall, the HR simulation is consistent with observations, in terms of the position of the northern extension and, to a lesser degree, the shedding periods. In particular, the model-simulated LC sheds rings in a nonperiodic manner, which is similar to what is observed. This result, together with the good agreement in other LC characteristics between HR and the observations, is remarkable for a coupled climate model.

We now examine the performance of the model simulations in representing the GoM SST field. Long-term time-averaged SST from observations shows intrusion of warm water into the southeastern GoM (Figure 1f) from the Caribbean Sea, which is caused by the LC. The temperature in the Caribbean Sea is approximately 3°C warmer than in the northern GoM on average. This pattern is also clearly seen in HR albeit SSTs tend to be warmer than observed in this simulation and the SST gradient sharper (Figure 1g). Although LR also shows significant SST contrast between the Caribbean Sea and the GoM, the gradient is significantly broader and does not exhibit a LC-related tongue as observed in the real ocean (Figure 1h).

Substantial SST variability is seen in both observations and HR simulation along the northern and eastern GoM coasts and in the deep eastern GoM (Figures 1i and 1j). High SST variability along the coasts is likely due to the influence of continental air and shallow water, especially on the wide West Florida shelf, while variability of the LC and rings is clearly responsible for SST fluctuations in the interior of GoM. This SST variability is well represented in HR, despite a slightly larger amplitude compared with observations. LR, on the other hand, is unable to capture any of the above mentioned SST variability (Figure 1k).

4. Air-Sea Interactions and Oceanic Lateral Advection

Over the central eastern GoM, significant positive correlation between SST anomalies and latent heat flux (LHF) anomalies out of the ocean is seen in observations (Figure 2a) and in HR (Figure 2b) [see also *Kirtman et al*., 2012]. Note that monthly anomalies here are obtained by removing climatological mean and seasonal cycle. Variations in the sensible heat fluxes are smaller but of the same sign as the LHF anomalies (not shown). This is indicative of warm SST associated with, for example, the LC and LC rings, resulting in the heat loss to the atmosphere (positive LHF). Similar positive correlation is observed in other parts of the ocean where the mesoscale variability is strong, such as the Southern Ocean, as well as the Gulf Stream and Kuroshio current systems [*Kirtman et al*., 2012]. In contrast, LR shows a negative correlation (Figure 2c), which suggests the atmosphere driving the SST variability [*Cayan*, 1992] by, for example, intrusion of warm Caribbean air into the GoM or winds enhancing latent heat flux out of the ocean and thus cooling SST. The difference between the two simulations suggests that the distribution of heat and SST in HR is driven in large part by upper ocean processes at short spatial scales, such as mesoscale advection and vertical entrainment, rather than the large-scale advection or atmospheric variability which one expects with LR.

We next examine the relationship between the variability in the upper ocean heat advection and LHF anomalies. Vertical advection and diffusion of heat were not available to us, so our analysis is focused on the lateral advection. To further reduce the influence of vertical processes, we define the upper ocean heat content as

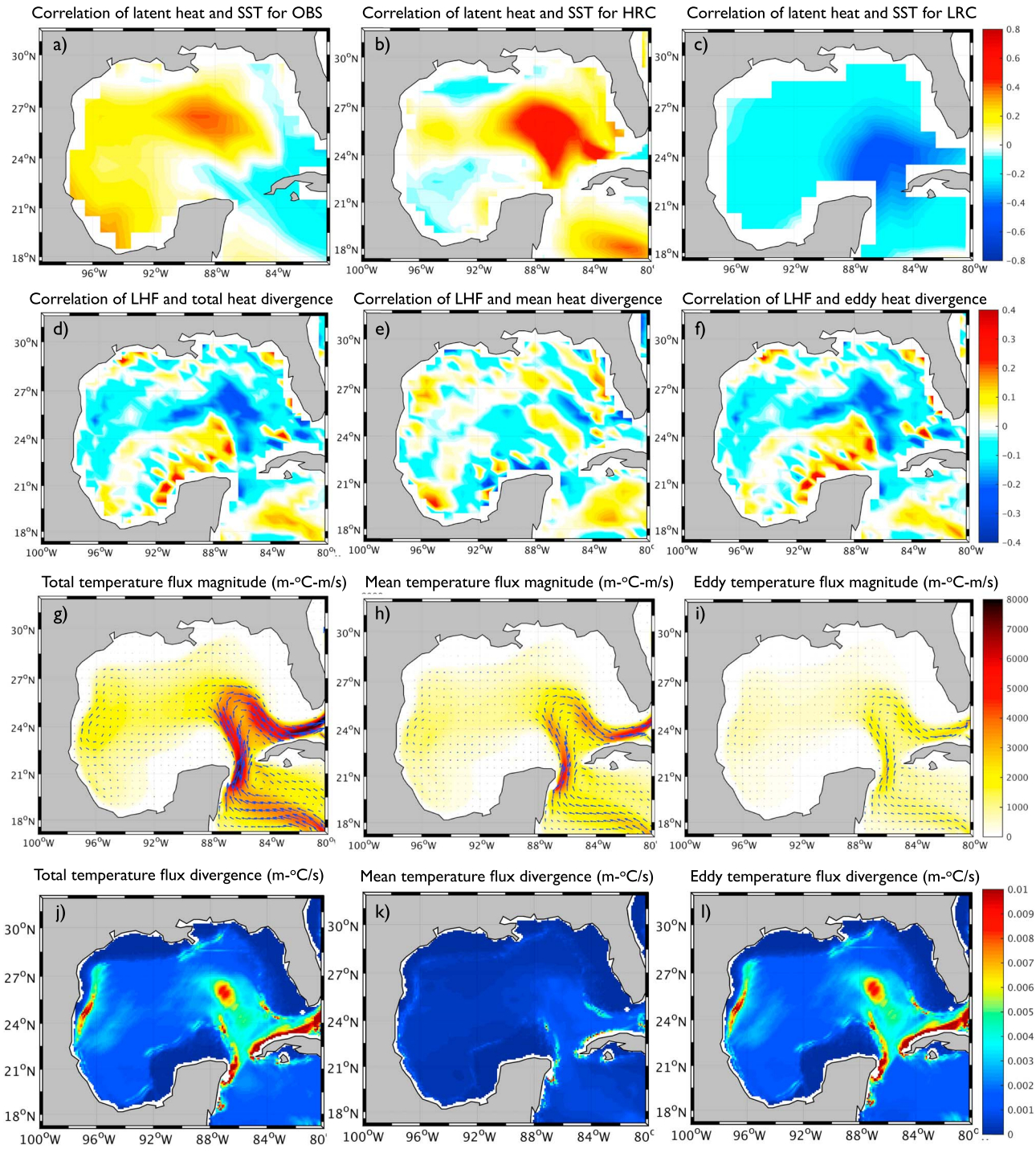

Figure 2. Correlation of latent heat flux and SST for (a) observations, (b) HR, and (c) LR. For HR, correlation of LHF with upper 200 m ocean: (d) total heat divergence, (e) mean heat divergence, and (f) eddy heat divergence. The 54 year mean of integrated upper 200 m temperature flux: direction (arrows) and magnitude (color; units are m-°C-m/s) for (g) total, (h) mean, and (i) eddy components. Standard deviation of monthly anomalies of integrated upper 200 m temperature flux divergence (m-°C/s) for (j) total, (k) mean, and (l) eddy components.

the integral of temperature over the top 200 m and integrate the lateral advection over the same depth. Mixed-layer entrainment, therefore, does not directly affect the heat content distribution, since winter mixed-layer depth in this region does not typically go deeper than about 125 m [*Muller-Karger et al.*, 2015]. The vertically integrated lateral heat divergence is negatively correlated with the LHF anomalies out of the

ocean (Figure 2d) in most of the region where SST and LHF anomalies are positively correlated. The largest correlation (up to −0.3) is observed along the northernmost boundary of the LC and in the vicinity of LC ring formation. West of the LC path, the correlation changes sign and it is positive along the Campeche Bank. In this region, the circulation is weak and upper ocean heat content anomalies are caused by the atmosphere, which explains the positive correlation. Subgrid diffusion of heat is negligible in HR.

Next, we show that lateral eddy-induced heat fluxes play a key role in heat distribution and air-sea interactions in the HR simulation. We take an approach similar to Reynolds decomposition and define "eddy" (fast varying) anomalies $\boldsymbol{u}'$ and T' as deviations from slowly evolving (mean) fields, $\langle \boldsymbol{u} \rangle$ and $\langle T \rangle$,

$$T' = T - \langle T \rangle; \quad \boldsymbol{u}' = \boldsymbol{u} - \langle \boldsymbol{u} \rangle$$

The operator $<\ldots>$ is a sliding mean over an integer number of months. From the model, we have only access to monthly values of temperature $\overline{T}$, horizontal velocities $(\overline{u}, \overline{v})$, and horizontal temperature fluxes $(\overline{uT}, \overline{vT})$, where the overline denotes monthly values. If we define the total temperature flux as $F = \langle \overline{\boldsymbol{u}T} \rangle$, we can calculate the mean F_{mean} and eddy F_{eddy} temperature fluxes as residual:

$$F_{\text{mean}} = \langle \overline{\boldsymbol{u}} \rangle \langle \overline{T} \rangle, \qquad F_{\text{eddy}} = \langle \overline{\boldsymbol{u}T} \rangle - \langle \overline{\boldsymbol{u}} \rangle \langle \overline{T} \rangle$$

If $<\ldots>$ is the 1 month mean, then by construction $F_{\text{eddy}} = \langle \boldsymbol{u}'T' \rangle$, but for longer averaging intervals the expression includes additional terms. The choice of the averaging interval is not straightforward. The 1 month average can attribute intermonthly mesoscale variability to the mean advection, whereas long averages can smear important features of the mean circulation, such as the LC and propagating LC rings. We tested the sensitivity of F_{eddy} and F_{mean} and their divergences to the averaging periods in $<\ldots>$ of 1, 3, 7, and 9 months. We found that F_{eddy} values are qualitatively the same, as long as the averaging is shorter than 1 year, but that longer averages indeed tend to diffuse important features, such as the LC and LC rings. This result implies that intermonthly variability has a much smaller impact on F_{eddy} than the submonthly fluctuations. In the rest of the study, F_{eddy} values are defined as submonthly anomalies. Note that these submonthly fluctuations are different from transient anticyclonic features, such as LC rings and northern part of the extended LC; these features are described as mean circulation in this study, because their typical time scale is of a few months.

We analyze mean (F_{mean}), eddy (F_{eddy}), and full heat fluxes, integrated over the upper 200 m. We estimate the correlation between each of these terms and monthly LHF anomalies in order to reveal their role in air-sea interactions (Figures 2d and 2f). Note, however, that a large correlation does not necessarily mean a dominance in the heat budget. The eddy heat flux divergence is strongly negatively correlated with monthly LHF out of the ocean, and the correlation patterns are very similar to those for the full advection (Figures 2d and 2f). In contrast, the correlation of the mean heat flux divergence and surface LHF is weak and has very different spatial distribution (Figure 2e).

The above analysis suggests that submonthly anomalies drive air-sea heat exchanges and that variability in the corresponding eddy heat fluxes explains variability in the LHF anomalies. At first sight, these results may seem counterintuitive since it is the mean LC that brings in warm waters from the Caribbean Seas and fuels warm anomalies and surface fluxes. This interpretation is perpetuated by a larger magnitude of the long-term time-mean F_{mean} compared to the magnitude of F_{eddy} (Figures 2g–2i), but it is the flux divergence and not the flux itself that affects surface fluxes. Indeed, the variability of monthly anomalies of F_{eddy} divergence is significantly larger than the variability of F_{mean} divergence and dominates the variability of monthly anomalies of the full lateral advection (Figures 2j–2l). In addition, the high variability of the lateral heat flux divergence occurs in the regions where there is high SST variability (Figure 1j) and high SST-LHF correlation (Figure 2b).

To summarize, our analysis demonstrates that eddy-induced heat flux divergence strongly modulates the air-sea exchanges of latent heat over the LC extension and LC rings. We next turn our attention to the mechanisms of the air-sea interactions over the LC extension and rings.

5. Air-Sea Interactions Over LC Rings and the LC Extension

Both the transient LC meanders and rings have circular anticyclonic rotation (although the LC meanders are not closed) and can be identified using the Okubo-Weiss parameter and positive sea surface height

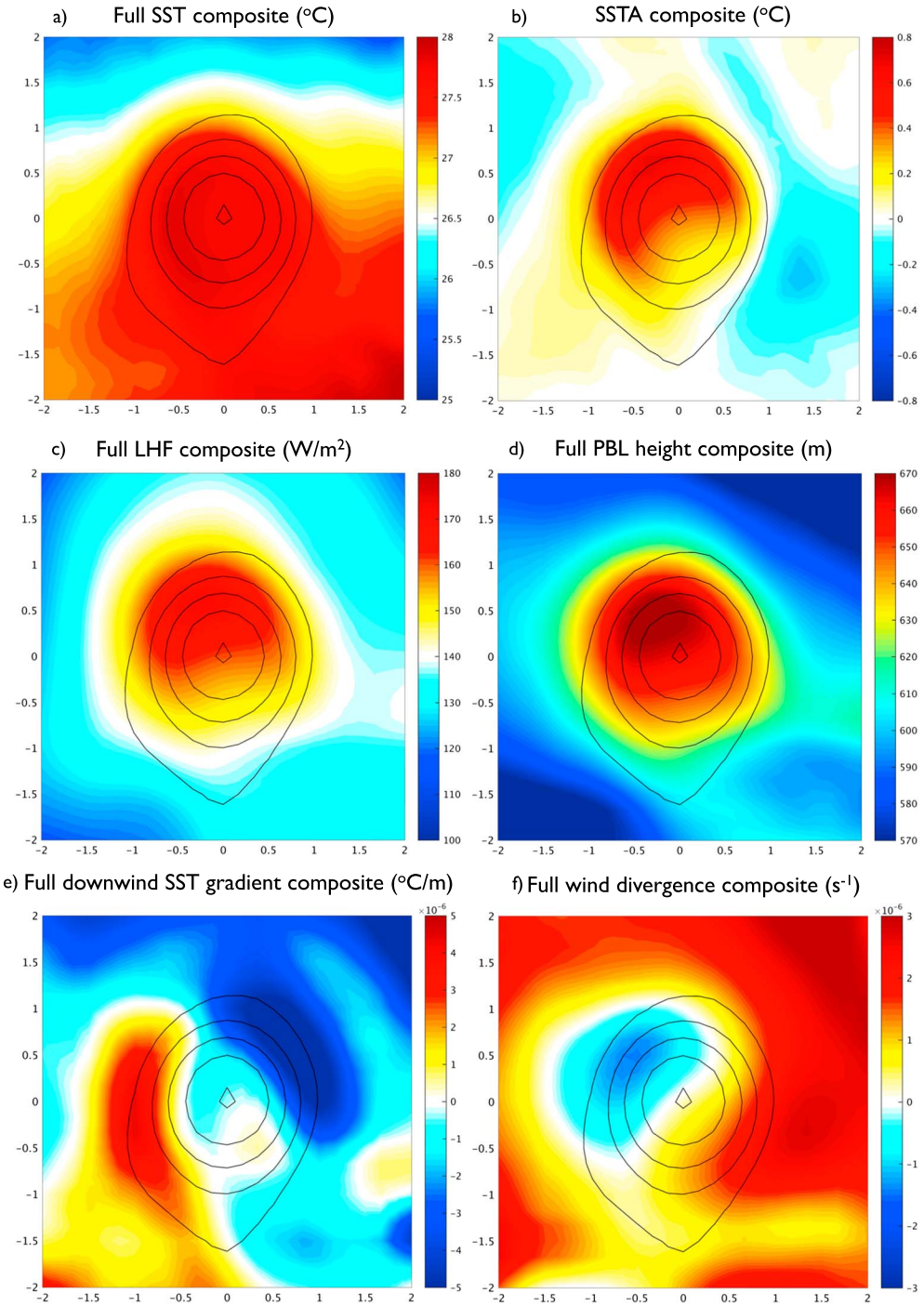

Figure 3. Averaged composites of anticyclones (LC meanders and LCEs) scaled to individual eddy radius with contours of sea level anomaly at 1, 10, 20, 30, and 40 cm. Abscissa and ordinate are eddy radius length. Plotted are composite of (a) full SST field (°C), (b) SST anomalies (°C), (c) full latent heat flux out of the ocean (W/m^2), (d) full atmospheric boundary layer height (m), (e) full downwind SST gradient (°C/m), and (f) full wind divergence (s^{-1}).

anomalies following *Faghmous et al.* [2015]. Over 54 years of monthly data from HR, we identify over 1100 monthly snapshots of anticyclonic features ("anticyclones" hereafter) that are larger than 10,000 km^2 and amplitude anomalies greater than 15 cm. Hence, there are usually two anticyclones in each monthly field: one associated with the transient LC meander and the other with a propagating LC ring. Note that we do not attempt to track individual patterns, and, for example, the same LC ring can appear in several

snapshots. Typical properties of these features are determined by the averaged composite of identified anticyclones. These anticyclones have a mean diameter of about 350 km and are associated with the intrusion of warm water into the GoM (Figure 3a).

The warm SST anomalies associated with these anticyclones are not symmetric with respect to the center. Instead, a typical anomaly has a maximum in the northwest quadrant (Figure 3b). This pattern is consistent with the fact that waters are advected clockwise while being cooled by the atmosphere, that is, initial northward advection of a warm anomaly and its eventual downstream dissipation. The northward flow acting on the background meridional SST gradient thus leads to the warming on the northwest flank. As we will see below, the eddy heat fluxes explain a large part of this structure in SST. As a result of this asymmetry, the imprint of these SST anomalies on the atmosphere is also asymmetric (Figures 3c–3f and supporting information S1). For instance, the LHF out of the ocean and planetary boundary layer (PBL) height anomaly both reach their maxima northwest from the eddy center (Figures 3c and 3d). Physically, this suggests that the warm anomaly has a direct forcing on the atmosphere by enhancing LHF and convection that would deepen the PBL.

The warm SST anomaly can also affect surface atmospheric circulation, namely, surface wind divergence/convergence. As is briefly described in section 1, the vertical mixing mechanism [*Wallace et al*., 1989] and pressure adjustment mechanism [*Lindzen and Nigam*, 1987] are two main processes that explain how SST gradients and anomalies can influence the overlying atmospheric flow. The first mechanism is concerned with how warm anomalies decrease atmosphere stability, thus enhancing downward transfer of momentum from winds aloft to the surface and strengthen surface winds. Inversely, cold anomalies increase atmospheric stability, which weakens surface winds. The wind blowing along SST gradients can thus acquire anomalous surface wind divergence/convergence, while the cross-gradient winds acquire extra curl. The pressure adjustment mechanism is akin to tropical processes whereby warm (cold) anomalies induce low (high) sea level pressure anomalies, or maxima (minima) in the pressure Laplacian, and corresponding wind convergence (divergence). Both mechanisms are particularly important over the oceanic mesoscale fronts and eddies.

Over the GoM anticyclones, the downwind SST gradient pattern shows a dipole with positive values to the western side and negative values to the northeastern side (Figure 3e). If the vertical mixing mechanism is at work, then a similar dipole pattern in wind divergence (convergence) on the western (northeastern) side should be seen. However, surface wind convergence exhibits its maximum centered over the warm SST anomaly (Figure 3f) and collocates with the maxima in the Laplacian of sea level pressure anomalies (Figure S1b), which suggests that the pressure adjustment mechanism is dominant. This is further corroborated by the collocation of maxima in horizontal atmospheric moisture convergence at surface and at higher levels, up to at least 800 mb (Figure S1a). The convergence supports atmospheric convection and approximately 10–15% anomalous precipitation over the warm anomaly (Figure S1c). In essence, the warm SST anomaly associated with anticyclones induces surface wind and moisture convergence that fuels atmospheric convection, enhances surface LHF, deepens the atmospheric boundary layer, and augments convective precipitation. Note, however, that monthly fields can obscure the relationship between winds convergence and SST gradient if the variability in wind direction is strong [*O'Neill et al*., 2017]. The monthly winds over these anticyclones have speeds of 3–5 m s^{-1}, are generally easterly, and have a standard deviation in direction varying between 30° and 60°. Since synoptic wind variability in direction and speed can potentially be larger than the variability in the monthly winds, this means that vertical mixing mechanism can still be important on synoptic time scales.

The importance of oceanic heat advection in supporting warm SST anomalies is further illustrated by the composite analysis of the lateral heat advection. The vertically integrated lateral temperature flux is nearly annular (Figure S2a), but its divergence has a distinct dipolar pattern. Northwest of the anticyclone center, the lateral oceanic heat flux is convergent (Figure S2d), SST anomaly is warm (Figure 3b), and LHF is out of the ocean (Figure 3c). Here the advection heats warm waters within the anticyclone even further, creating a warm SST anomaly that modulates the air-sea interactions. In contrast, the divergent oceanic heat flux in the southeastern part of the anticyclone does not result in a negative SST anomaly (Figure 3b), and the atmospheric cooling is weak there (Figure 3c). This implies cooling of warm waters, which results in temperatures close to its background value (i.e., zero SST anomaly). Consistent with the regional analysis of the previous section, the oceanic heat flux within each anticyclone is dominated by the F_{mean} component (Figures S2b and S2c), but the flux divergence is dominated by F_{eddy} component (Figures S2e and S2f).

6. Summary and Discussion

This study examines the importance of oceanic mesoscale variability on atmospheric processes and air-sea interactions in the GoM. The LR simulation, which has similar resolution to current generation GCMs and does not resolve mesoscale processes, produces negative correlation between SST anomalies and LHF out of the ocean. This is in contrast to observations and the high-resolution (HR) coupled simulation that exhibit positive correlation between SST anomalies and ocean-to-atmosphere LHF, indicating the SST control on the air-sea exchanges of heat. These SST anomalies are generated by lateral advection of heat in the ocean, and this process triggers a substantial response within the atmospheric boundary layer. To examine the generation mechanism, we decomposed velocities and temperature into the slow-varying component (mean) and fast fluctuations (eddies). We find that while the magnitude of oceanic lateral fluxes by the mean currents is larger, the divergence of the eddy flux dominates the total lateral flux divergence. Combined with the high correlation between the oceanic eddy flux convergence and LHF out of the ocean, these results demonstrate the leading role of eddies in shaping the SST anomalies and modulating the air-sea interactions. Our composite analysis of the air-sea interactions over anticyclonic LC meanders and rings reveals a warm SST anomaly in the northwest portion of the anticyclone, which is sustained by the eddy flux convergence and imprints on surface turbulent heat flux, atmospheric circulation, and convective precipitation.

The LC is the dominant current in the GoM, with strong spatial variability on the scale on the order of 100 km (horizontal shear and ring formation) and temporal variability on the time scale of several months. These scales are traditionally associated with mesoscale, which complicates the definition of the mean circulation. Instead of separating mean and mesoscale, we decomposed GoM currents into the slow (LC and rings) and fast (eddies) fluctuations with submonthly time scales. This decomposition in time is clearly not unique, since the time scale separation between the mean and eddies is nearly nonexistent in the GoM. Nevertheless, the dominant role of submonthly eddies in the oceanic lateral heat convergence is a robust property regardless of the exact choice of decomposition. We did not carry out analysis of the dynamics and origins of submonthly processes in this study, since only monthly means were available to us. In the GoM, these processes include submesoscale motions and some mesoscale processes, such as eddies and filaments. While some of the LC frontal eddies have a signature at the monthly scale, others have periods shorter than 30 days [e.g., *Jouanno et al*., 2016]. Submonthly mesoscale processes also include fast fluctuations in LC meanders [*Donohue et al*., 2015], eddies away from the LC [*Hamilton et al*., 2002], and filaments at the shelf break [e.g., *Schiller et al*., 2011]. The model can resolve the mesoscale submonthly variability, but the monthly averaging of the outputs does not allow us to properly characterize them in the HR simulation. Further studies of the mechanisms of air-sea interactions and relevant variability need to be carried out in very high resolution, high frequency output coupled simulations and observational data sets.

In contrast, the meandering LC corresponds to nearly nondivergent oceanic heat flux and has a weaker local effect on the distribution of oceanic heat anomalies and air-sea interactions in the GoM. This secondary role of the mean advection is consistent with earlier model-based studies of large-scale advection of heat in the region [*Lee et al*., 2007]. This conclusion does not imply that the large-scale circulation is not important for heat budgets in the GoM. Submonthly fluctuations can be in large part produced by instability and variability of the LC and rings, and both types of motions are tightly linked dynamically. Conditions upstream of the GoM and large-scale characteristics of the LC inside the GoM can therefore influence the air-sea interactions at all scales. For instance, the LC variability and ring formation have been shown to depend on these large-scale properties and wind distribution in the Caribbean Seas [e.g., *Chang and Oey*, 2013]. Our results emphasize the importance of studying this connection.

This study emphasizes the importance of oceanic mesoscale variability in coupled atmosphere-ocean dynamics. Recent advances in computing power led to the emergence of global climate models with high spatial resolution in the oceans, capable of at least partially resolving the oceanic mesoscale. These simulations, combined with observational data sets, reveal new regimes of coupled dynamics, in which highly energetic ocean currents generate strong SST variability and can significantly modulate air-sea interactions and induce atmospheric response. Although more research on these regimes is needed for further understanding of coupled atmosphere-ocean processes, it is clear that air-sea interactions at oceanic mesoscale are capable

of influencing local climate and its variability and potentially have substantial remote influence on the climate of North America [*Jung and Kirtman*, 2016]. These processes need to be captured in order to improve fidelity of climate models and accuracy of their predictions.

Acknowledgments
Funding for this study is supported by the NOAA grant NA12OAR4310073. M. Le Hénaff received partial support for this work from the NOAA Atlantic Oceanographic and Meteorological Laboratory. B.P.K. acknowledges support from the National Science Foundation grant OCE1419569. We used model data output from CCSM4 that is on the University of Miami, Center for Computational Science machine named VISX. Model data sets are called HRC06 and LRC07 and can be made available upon request from the corresponding authors. The mapped altimetry products were produced by Ssalto/Duacs and distributed by Aviso, with the support from CNES (http://www.aviso.oceanobs.com/duacs). The MUR Global High-Resolution SST data set is distributed by NASA (http://podaac.jpl.nasa.gov/dataset/JPL-L4UHfnd-GLOB-MUR).

References

Bryan, F. O., R. Tomas, J. M. Dennis, D. B. Chelton, N. G. Loeb, and J. L. McClean (2010), Frontal scale air–sea interaction in high-resolution coupled climate models, *J. Clim.*, *23*, 6277–6291, doi:10.1175/2010JCLI3665.1.

Cayan, D. R. (1992), Latent and sensible heat flux anomalies over the northern oceans: Driving the sea surface temperature, *J. Phys. Oceanogr.*, *22*, 859–881.

Chang, Y.-L., and L.-Y. Oey (2013), Coupled response of the trade wind, SST gradient, and SST in the Caribbean Sea, and the potential impact on Loop Current's Interannual Variability*, *J. Phys. Oceanogr.*, *43*, 1325–1344, doi:10.1175/JPO-D-12-0183.1.

Chang, Y. L., and L. Y. Oey (2012), Why does the Loop Current tend to shed more eddies in summer and winter?, *Geophys. Res. Lett.*, *39*, L05605, doi:10.1029/2011GL050773.

Chelton, D. B., M. G. Schlax, and R. M. Samelson (2007), Summertime Coupling between Sea Surface Temperature and Wind Stress in the California Current System, *J. Phys. Oceanogr.*, *37*, 495–517, doi:10.1175/JPO3025.1.

Czaja, A (2012), Ocean-atmosphere coupling in midlatitudes: Does it invigorate or damp the storm track?, vol. 44, pp. 1–19. [Available at http://www.sp.ph.ic.ac.uk/~aczaja/pdf/ECMWF_Sept12.pdf.]

Donohue, K. A., D. R. Watts, P. Hamilton, R. Leben, M. Kennelly, and A. Lugo-Fernández (2015), Gulf of Mexico Loop Current path variability, *Dyn. Atmos. Oceans*, *76*, 174–194.

Dukhovskoy, D. S., R. R. Leben, E. P. Chassignet, C. A. Hall, S. L. Morey, and R. Nedbor-Gross (2015), Characterization of the uncertainty of loop current Metrics using a multidecadal numerical simulation and altimeter observations, *Deep Sea Res., Part I*, *100*, 140–158, doi:10.1016/j.dsr.2015.01.005.

Enfield, D. (2005), The heat balance of the western hemisphere warm pool, *J. Clim.*, *18*, 2662–2681, doi:10.1175/JCLI3427.1.

Faghmous, J. H., I. Frenger, Y. Yao, R. Warmka, A. Lindell, and V. Kumar (2015), A daily global mesoscale ocean eddy dataset from satellite altimetry, *Sci. Data*, *2*, 150028, doi:10.1038/sdata.2015.28.

Frenger, I., N. Gruber, R. Knutti, and M. Münnich (2013), Imprint of Southern Ocean eddies on winds, clouds and rainfall, *Nat. Geosci.*, *6*, 608–612, doi:10.1038/ngeo1863.

Hamilton, P., T. J. Berger, and W. Johnson (2002), On the structure and motions of cyclones in the northern Gulf of Mexico, *J. Geophys. Res.*, *107*(C12), 3208, doi:10.1029/1999JC000270.

Hewitt, H. T., et al. (2016), The impact of resolving the Rossby radius at mid-latitudes in the ocean: Results from a high-resolution version of the Met Office GC2 coupled model, *Geosci. Model Dev.*, *9*, 3655–3670, doi:10.5194/gmd-9-3655-2016.

Jacob, S. D., and L. K. Shay (2003), The role of oceanic mesoscale features on the tropical cyclone-induced mixed layer response: A case study, *J. Phys. Oceanogr.*, *33*, 649–676, doi:10.1175/1520-0485(2003)33<649:TROOMF>2.0.CO;2.

Jaimes, B., and L. K. Shay (2009), Mixed layer cooling in mesoscale oceanic eddies during Hurricanes Katrina and Rita, *Mon. Weather Rev.*, *137*, 4188–4207, doi:10.1175/2009MWR2849.1.

Jaimes, B., and L. K. Shay (2010), Near-inertial wave wake of Hurricanes Katrina and Rita over mesoscale oceanic eddies, *J. Phys. Oceanogr.*, *40*, 1320–1337, doi:10.1175/2010JPO4309.1.

Jouanno, J., J. Ochoa, E. Pallàs-Sanz, J. Sheinbaum, F. Andrade-Canto, J. Candela, and J. M. Molines (2016), Loop current frontal eddies: Formation along the Campeche Bank and impact of coastally trapped waves, *J. Phys. Oceanogr.*, *46*(11), 3339–3363.

Jung, E., and B. P. Kirtman (2016), Can we predict seasonal changes in high impact weather in the United States?, *Environ. Res. Lett.*, *11*, 1–8, doi:10.1088/1748-9326/11/7/074018.

Kirtman, B. P., et al. (2012), Impact of ocean model resolution on CCSM climate simulations, *Clim. Dyn.*, *39*, 1303–1328, doi:10.1007/s00382-012-1500-3.

Leben, R. R. (2005), Altimeter-derived loop current Metrics, in *Circulation in the Gulf of Mexico: Observations and Models*, edited by W. Sturges and A. Lugo-Fernandez, pp. 181–201, AGU, Washington, D. C., doi:10.1029/161GM15.

Lee, S.-K., D. B. Enfield, and C. Wang (2007), What drives the seasonal onset and decay of the western hemisphere warm pool?, *J. Clim.*, *20*, 2133–2146, doi:10.1175/JCLI4113.1.

Le Hénaff, M., V. H. Kourafalou, R. Dussurget, and R. Lumpkin (2014), Cyclonic activity in the eastern Gulf of Mexico: Characterization from along-track altimetry and in situ drifter trajectories, *Prog. Oceanogr.*, *120*, 120–138, doi:10.1016/j.pocean.2013.08.002.

Lindzen, R. S., and S. Nigam (1987), On the role of sea surface temperature gradients in forcing low-level winds and convergence in the tropics, *J. Atmos. Sci.*, *44*, 2418–2436.

Muller-Karger, F. E., et al. (2015), Natural variability of surface oceanographic conditions in the offshore Gulf of Mexico, *Prog. Oceanogr.*, *134*, 54–76.

McClean, J. L., et al. (2011), A prototype two-decade fully-coupled fine-resolution CCSM simulation, *Ocean Model.*, *39*, 10–30, doi:10.1016/j.ocemod.2011.02.011.

O'Neill, L. W., D. B. Chelton, and S. K. Esbensen (2012), Covariability of surface wind and stress responses to sea surface temperature fronts, *J. Clim.*, *25*, 5916–5942, doi:10.1175/JCLI-D-11-00230.1.

O'Neill, L., T. Haack, D. Chelton, and E. Skyllingstad (2017), The Gulf Stream Convergence Zone in the time-mean winds, *J. Atmos. Sci.*, doi:10.1175/JAS-D-16-0213, in press.

Oey, L., T. Ezer, and H. Lee (2005), Loop current, rings and related circulation in the Gulf of Mexico: A review of numerical models and future challenges, in *Circulation in the Gulf of Mexico: Observations and Models*, vol. 161, edited by W. Sturges and A. Lugo-Fernandez, pp. 31–56, AGU, Washington, D. C., doi:10.1029/161GM04.

Putrasahan, D., B. Kirtman, and L. M. Beal (2015), Modulation of Agulhas leakage SST interannual variability associated with ENSO, *J. Clim.*, doi:10.1175/JCLI-D-15-0172.1, in press.

Putrasahan, D. A., A. J. Miller, and H. Seo (2013), Isolating mesoscale coupled ocean–atmosphere interactions in the Kuroshio extension region, *Dyn. Atmos. Oceans*, *63*, 60–78, doi:10.1016/j.dynatmoce.2013.04.001.

Reynolds, R. W., T. M. Smith, C. Liu, D. B. Chelton, K. S. Casey, and M. G. Schlax (2007), Daily high-resolution-blended analyses for sea surface temperature, *J. Clim.*, *20*, 5473–5496, doi:10.1175/2007JCLI1824.1.

Schiller, R. V., V. H. Kourafalou, P. Hogan, and N. D. Walker (2011), The dynamics of the Mississippi River plume: Impact of topography, wind and offshore forcing on the fate of plume waters, *J. Geophys. Res.*, *116*, C06029, doi:10.1029/2010JC006883.

Shay, L. K., G. J. Goni, and P. G. Black (2000), Effects of a warm oceanic feature on Hurricane Opal, *Mon. Weather Rev.*, *128*, 1366–1383, doi:10.1175/1520-0493.

Siqueira, L., and B. P. Kirtman (2016), Atlantic near-term climate variability and the role of a resolved Gulf Stream, *Geophys. Res. Lett.*, *43*, 3964–3972, doi:10.1002/2016GL068694.

Small, R. J., et al. (2008), Air-sea interaction over ocean fronts and eddies, *Dyn. Atmos. Oceans*, *45*, 274–319, doi:10.1016/j.dynatmoce.2008.01.001.

Souza, J. M. A. C., B. Chapron, and E. Autret (2014), The surface thermal signature and air–sea coupling over the Agulhas rings propagating in the South Atlantic Ocean interior, *Ocean Sci.*, *10*, 633–644, doi:10.5194/os-10-633-2014.

Vukovich, F. M. (2007), Climatology of ocean features in the Gulf of Mexico, *Bull. Am. Meteorol. Soc.*, *88*, 156–157, doi:10.1175/JPO2989.1.

Wallace, J. M., T. P. Mitchell, and C. Deser (1989), The influence of sea-surface temperature on surface wind in the eastern equatorial Pacific: Seasonal and interannual variability, *J. Clim.*, *2*, 1492–1499, doi:10.1175/1520-0442(1989)002<1492:TIOSST>2.0.CO;2.

Wang, C., and D. B. Enfield (2002), A further study of the tropical western hemisphere warm pool, *Phys. Oceanogr.*, *16*, 1476–1493, doi:10.1175/1520-0442-16.10.1476.

Wang, C., and S. K. Lee (2007), Atlantic warm pool, Caribbean low-level jet, and their potential impact on Atlantic hurricanes, *Geophys. Res. Lett.*, *34*, L02703, doi:10.1029/2006GL028579.

Wang, C., and S. K. Lee (2008), Global warming and United States landfalling hurricanes, *Geophys. Res. Lett.*, *35*, L02708, doi:10.1029/2007GL032396.

Wang, C., D. B. Enfield, S. K. Lee, and C. W. Landsea (2006), Influences of the Atlantic warm pool on western hemisphere summer rainfall and Atlantic hurricanes, *J. Clim.*, *19*, 3011–3028, doi:10.1175/JCLI3770.1.

Wang, C., S. Lee, and D. B. Enfield (2007), Impact of the Atlantic warm pool on the summer climate of the western hemisphere, *J. Clim.*, *20*, 5021–5040, doi:10.1175/JCLI4304.1.

Yu, L., and R. A. Weller (2007), Objectively analyzed air-sea heat fluxes for the global ice-free oceans (1981-2005), *Bull. Am. Meteorol. Soc.*, *88*, 527–539, doi:10.1175/BAMS-88-4-527.